C.P. No. 891

MINISTRY OF AVIATION

AERONAUTICAL RESEARCH COUNCIL

CURRENT PAPERS

The Performance of a Conical Convergent-Divergent Nozzle with Area Ratio 2.9 in External Flow

By

G. T. Golesworthy and M. V. Herbert

LONDON: HER MAJESTY'S STATIONERY OFFICE

1966

SIX SHILLINGS NET

U.D.C. No. 621-225.1:533.691.18

C.P. No. 891
November 1963

The performance of a conical convergent-divergent* nozzle with area ratio 2.9 in external flow

- by -

G. T. Golesworthy and M. V. Herbert

SUMMARY

A model internal-expansion propelling nozzle with conical divergence of 10° semi-angle, area ratio 2.9 (design pressure ratio 20), parallel afterbody and thin annular base, has been tested both in quiescent air and in external flow over the range of Mach number 0.7 to 2.4. Measurements have been made of nozzle base pressure, and thrust efficiencies derived with reference to both ambient and base pressure levels. Internal thrust efficiencies with external flow agree with those in quiescent air, provided that the boundary layer is in the same state in both cases.

*Replaces N.G.T.E. M.371 - A.R.C.26 491

CONTENTS

ILLUSTRATIONS

1.0 Introduction

Current interest in supersonic transport aircraft raises many questions concerning propelling nozzle performance. In this context it is valuable to know just how good an efficiency can be obtained from a simple convergent-divergent de Laval type of nozzle throughout the range of typical operating conditions. Simulation of external flow is clearly essential, in that a representative base pressure must be applied, as this will determine the nozzle internal expansion conditions. On present knowledge, theoretical prediction of base pressure is in many cases unreliable, and experimental measurements have therefore been undertaken.

The system adopted was for simplicity of testing axisymmetric, with a parallel afterbody and the smallest practicable base area, so as to correspond with an installation having as high a level of base pressure as possible.

2.0 Description of test equipment

The external flow rig used for these tests had two alternative working sections as shown in Figure 1, with common supply and exhaust arrangements. Each line comprised a nozzle, viewing section and pressure recovery diffuser. The upper or transonic line gave external flow Mach numbers in the range 0.7 to 1.5, and the lower or supersonic line covered the range 1.3 to 2.4. Test models were carried on a long parallel hollow sting, passing through the throat of the test line nozzles, and this sting assembly could be interchanged between the two external flow lines and a quiescent air line as desired.

Figures 2 and 3 show the arrangement of the sting carrier section, which fitted immediately ahead of either external flow nozzle, and consisted of a round duct with a streamlined bullet carried on its centreline by a single hollow arm. From the bullet the sting, with the model on its downstream end, was supported so as to locate the outlet plane of the model in the window of the viewing section. An inner load-carrying tube delivered air to the model, controlled externally, and instrumentation lines from the model passed between the inner tube and outer cover of the sting.

The transonic line was equipped with a slotted nozzle of circular cross-section, 11.3 in. diameter (Figure 2), whose outlet Mach number could be varied simply by adjustment of the pressure ratio applied to the nozzle. Calibration of a similar system[1] had shown that good distribution could be obtained with a sting in position up to Mach number 1.4, and in the present work no disturbing effects were observed at 1.5.

For the supersonic line a two-dimensional flexible wall nozzle was used with 12 in. × 12 in. outlet, which had nominal design Mach number limits of 1.3 and 3.5 (Figure 3). With the sting present, however, throat blockage imposed an upper limit of 2.6. This nozzle had been tested previously with a dummy sting[2], and found to give distortions, based on sidewall static pressure, of less than 1.3 per cent of the mean Mach number in the working section for Mach numbers between 1.5 and 2.2. The Mach number distribution obtained from traverses in the freestream was better than this figure.

Tests in quiescent air were carried out by enclosing the end of the sting in a depression chamber, to which was connected a diffuser system for pressure recovery (Figure 4).

Figures 5 and 6 show the geometry of the test model. Throat diameter was 2.000 in., nominal design pressure ratio 20, and the ratio plane exit area/geometric throat area was 2.90. Approach and divergent semi-angles were 10°, and a radius of curvature of 1.0 in. blended the two conical sections at the throat. The model afterbody was continued parallel up to the outlet plane, forming a narrow annular base 0.050 in. wide.

3.0 Instrumentation and air supplies

No thrust measuring equipment was fitted in this test rig, and model internal gross thrust was derived from:-

(i) Knowledge of discharge coefficient (C_D), obtained from tests on a quiescent air rig equipped for mass flow measurement. When choked, this model was found to have $C_D = 0.991$.

(ii) Calculated stream thrust at the throat plane.

(iii) Measurement of pressures along the divergent portion of the nozzle.

(iv) Measurement of base pressure.

(v) Computed allowance for friction.

The expression for gross thrust efficiency* was derived in Reference 3:-

$$\eta_F = \frac{1.26789\ C_D.\mu + \int_1^{A_e/A_g} \frac{P_w}{P_t}\, d\left(\frac{A}{A_g}\right) - \frac{1}{R}.\frac{A_e}{A_g} - \phi}{0.012316\ C_D\left[\frac{v}{\sqrt{T_t}}\right]_R}$$

taking $\gamma = 1.4$,

where μ = vacuum stream thrust efficiency at the throat, taken to be 1.003 when choked as in Reference 5 for similar throat geometry†

In accordance with the argument presented in Reference 3, no correction for "real air" effects has been applied.

* For definition see Appendix

† Radius of throat curvature = ½ throat diameter

Pressure instrumentation on the model accordingly consisted of:-

(i) A rake of 7 pitot tubes 1 mm o.d. at entry, spaced on an equal-area basis.

(ii) Eleven static tappings spirally positioned down the divergent section, each 0.020 in. diameter.

(iii) Two tappings spaced 90° apart in the base annulus.

(iv) Two static tappings on the external surface.

Each test line nozzle was fitted with wall pressure tappings, and these were considered to be more reliable in assessment of external Mach number than the model afterbody tappings.

Air supply temperature to both model and test line nozzle was maintained within the range 25 to 35°C at all times, and no further attention was paid to temperature measurement. Air dryness was measured by an R.A.E.-Bedford pattern frost-point hygrometer, and held at better than -20°C throughout.

Supply pressure was at a level of 5 atmospheres, and throttled independently as required for model and external flow lines.

4.0 Model operating conditions

The following values of external Mach number were chosen:-

(i) Supersonic line: M_∞ = 1.5, 1.75, 2.0, 2.4.

(ii) Transonic line: M_∞ = 0.7, 0.9, 1.1, 1.3, 1.5.

At each Mach number the model was tested over a representative band of exhaust pressure ratio (E.P.R.) within the limits 2 and 20, except in the quiescent case where tests covered the whole of this range.

5.0 Model performance

5.1 Base pressure

This quantity, which controls the performance of an internal-expansion nozzle of given geometry, results from the interaction of the internal and external flows which meet at the nozzle outlet. From theoretical considerations, boundary layer thicknesses are known to be of great importance in determining conditions in this mixing region and hence the base pressure itself, as is also the thickness of base separating the two streams, round which they have to bend. In practical installations, where large base areas are likely to be avoided, the thickness of the external boundary layer is generally much greater than that of the internal, so that the former becomes a dominant quantity in the control of base pressure.

In the present test arrangement, a somewhat unnaturally thick outer boundary layer was produced by the long length of parallel sting tube on which the model was mounted. Measurements made in the freestream suggested a boundary layer height of around $\frac{3}{4}$ in. on the outer surface of the model in both external flow lines and at all values of Mach number:

this height is 21 per cent of the model outer diameter. An engine nacelle might be expected to grow a boundary layer perhaps 12 per cent of its diameter by the nozzle outlet plane, so that base pressures in practice would tend to be rather lower than those measured here.

The effect of base pressure is two-fold. First, by depressing below ambient the pressure to which the nozzle is exhausting, it causes a higher pressure ratio to be applied across the nozzle for a given inlet total pressure. Although the nozzle internal efficiency, based on applied pressure ratio (A.P.R.), may in consequence be increased, the net effect is a loss of performance. This can be realised by considering how much more of the divergent walls of the nozzle are subjected to a pressure below ambient. Secondly, there will be a higher drag on the base area itself.

In the expression for thrust efficiency given in Section 3.0, no account is taken of this base drag term. Efficiency may thus be computed in terms of either A.P.R. or E.P.R. at will, depending which value is used for the quantity R. The two forms of efficiency are related by the symmetrical equation,

$$\eta_{F(EPR)} \frac{K}{g}\left[\frac{v}{\sqrt{T_t}}\right]_{EPR} + \frac{A_e}{A^*}\cdot\frac{1}{E.P.R.} = \eta_{F(APR)} \frac{K}{g}\left[\frac{v}{\sqrt{T_t}}\right]_{APR} + \frac{A_e}{A^*}\cdot\frac{1}{A.P.R.}$$

where K = 0.3966 in these tests. In the case of an internal expansion nozzle, the efficiency based on A.P.R. would be expected to be independent of M_∞, as it is a function only of internal flow conditions, and as such could be determined from tests on a quiescent air rig. But the aircraft project engineer, who generally knows only the E.P.R. and M_∞, requires his efficiency to be based upon E.P.R. The link between these features is, of course, a knowledge of base pressure.

Two ways of presenting this have been used. Figure 7 gives the ratio $\frac{P_b}{P_\infty}\left(=\frac{E.P.R.}{A.P.R.}\right)$, and Figure 8 the base pressure coefficient, in both cases as functions of E.P.R. and M_∞. It will be observed that in Figure 7 the curve for each value of M_∞ drops abruptly, implying a large change in A.P.R. for a quite small variation in E.P.R. Thereafter all results lie within a common and fairly narrow band, $\frac{P_b}{P_\infty}$ increasing gradually in level with E.P.R. Corresponding to this band is the limiting curve of base pressure coefficient in Figure 8.

5.2 Internal pressures

Typical internal pressure distributions are shown in Figures 9 to 11 for a range of A.P.R. in each of the three test arrangements. Differences in separation pattern between the three figures are associated with the fact that the level of model inlet total pressure corresponding to any particular A.P.R. varied in each system according to the different pressure recovery characteristics. In general, the highest levels of P_t occurred in the quiescent air test line, and the lowest with supersonic external flow. For any one system and Mach number, P_t increased

approximately in proportion to E.P.R. Values of throat Reynolds number (proportional to P_t) appear in Figure 12, on which is also marked the level at 1.0 million below which the boundary layer in a nozzle of this type is thought not to be fully turbulent[4]. It can be seen that in this category lie all the supersonic test line results below A.P.R. 14, some of the transonic test line results below A.P.R. 4, and none of the quiescent line results. Reference to Figures 9 to 11 indicates good correspondence between the division marked in Figure 12 and the forms of separation pattern observed.

5.3 Thrust efficiency

Turning to Figure 13, the efficiency based on E.P.R. is seen to depart less and less readily from the "running full" line as M_∞ is increased, reflecting the reduction in base pressure ratio (see Figure 7). The inflection or "wiggle" in some of the curves occurs during the abrupt fall in $\frac{P_b}{P_\infty}$ already noted.

Across the plot of Figure 13 could be drawn an engine operating line, connecting E.P.R. with M_∞ for any particular project. It is likely that for the acceleration phase of a typical flight plan such a characteristic would, very approximately, run level at around 80 per cent efficiency to meet the "running full" line, and thereafter follow it up to the design point.

In calculating the values of η_F according to the equation given in Section 3.0, an estimate must be made of the amount to be deducted for friction. Curves are available[5] of quantities termed the "momentum loss" and "displacement loss", whose sum represents the net deduction required in this case. Unfortunately, the changing level of throat Reynolds number and the rather uncertain state of the boundary layer introduce complications. The effect on friction of transition and of Reynolds number as such tend, however, to be opposite in sense, and for simplicity a constant correction of 0.70 per cent has been applied throughout, this value being appropriate to the design-point operating conditions.

Efficiencies based on A.P.R. are shown in Figure 14. The same friction allowance has been incorporated as in Figure 13, and the design-point levels of efficiency are the same. At low pressure ratios, the situation is largely controlled by the effect of boundary layer conditions on separation, according to Figure 12. For comparison, on Figure 14 have been included two curves:-

(i) taken from Reference 5, where an essentially identical nozzle with laminar boundary layer was tested on a quiescent air rig equipped for thrust measurement;

(ii) the quiescent air results taken from Figure 13, for which the boundary layer is beyond doubt turbulent (see Figures 11 and 12).

Inspection then reveals that those external flow points which, from Figure 12, would be expected to be turbulent, do in fact lie fairly well around the appropriate curve in Figure 14. It may be observed that only in the range of A.P.R. 5 to 11 is there any large difference in efficiency level as between the curves for laminar and turbulent separation (Figure 14), and reference to Figure 12 shows that almost no experimental

points exist in this range for which the boundary layer would be expected to be other than turbulent. This results from the circumstance, already noted, that with external flow the A.P.R. changes very rapidly within a certain band for quite small variation of E.P.R., and this band happens to correspond more or less to the range in which the laminar and turbulent curves differ most widely. Elsewhere, differences are masked by the experimental scatter in Figure 14; and any trend, as for instance from laminar efficiency level at low A.P.R. to turbulent at high as would be suggested by Figure 12, is difficult to detect. Reverting to Figure 13, it is worth noting that of the data shown almost none are other than turbulent, since the laminar results gave very low efficiencies based on E.P.R. which are not shown on the graph.

It is of interest to compare the design-point efficiency of 0.991[*] from Figures 13 and 14 with that obtained from the thrust rig[5]. A design-point figure of 0.990 was there obtained, with a laminar boundary layer and low Reynolds number, hence a reduced friction loss. Making allowance for these effects, the comparable thrust rig answer would be 0.9882. Although in general it is thought that accuracy better than $\frac{1}{2}$ per cent should not be claimed for pressure plotting methods, the standard of agreement in this particular case is quite good.

It should be noted that curves of both $\eta_{F(APR)}$ and $\eta_{F(EPR)}$ peak when the appropriate pressure ratio (either A.P.R. or E.P.R.) is equal to the nozzle design pressure ratio, that is to say when the nozzle is correctly expanded to the reference pressure, be it either P_b or P_∞. Similarly, the "running full" line (η versus pressure ratio) is independent of which pressure ratio is used.

When employing these test results in the form $\eta_{F(EPR)}$, it should be remembered that no allowance is included for the drag force on the annular base. If an overall external efficiency is required for comparison with other systems, as for instance any arrangement incorporating base bleed, then a quantity $\Delta\eta$ must be deducted from $\eta_{F(EPR)}$, given by

$$\Delta\eta = \frac{\frac{A_b}{A^*}\left(\frac{1}{E.P.R.} - \frac{1}{A.P.R.}\right)}{\frac{k}{g}\left[\frac{v}{\sqrt{T_t}}\right]_{EPR}}$$

where A_b is the annular base area. Values of $\Delta\eta$ are given in Figure 15.

[*] 0.998 before correction for friction

FIG.6

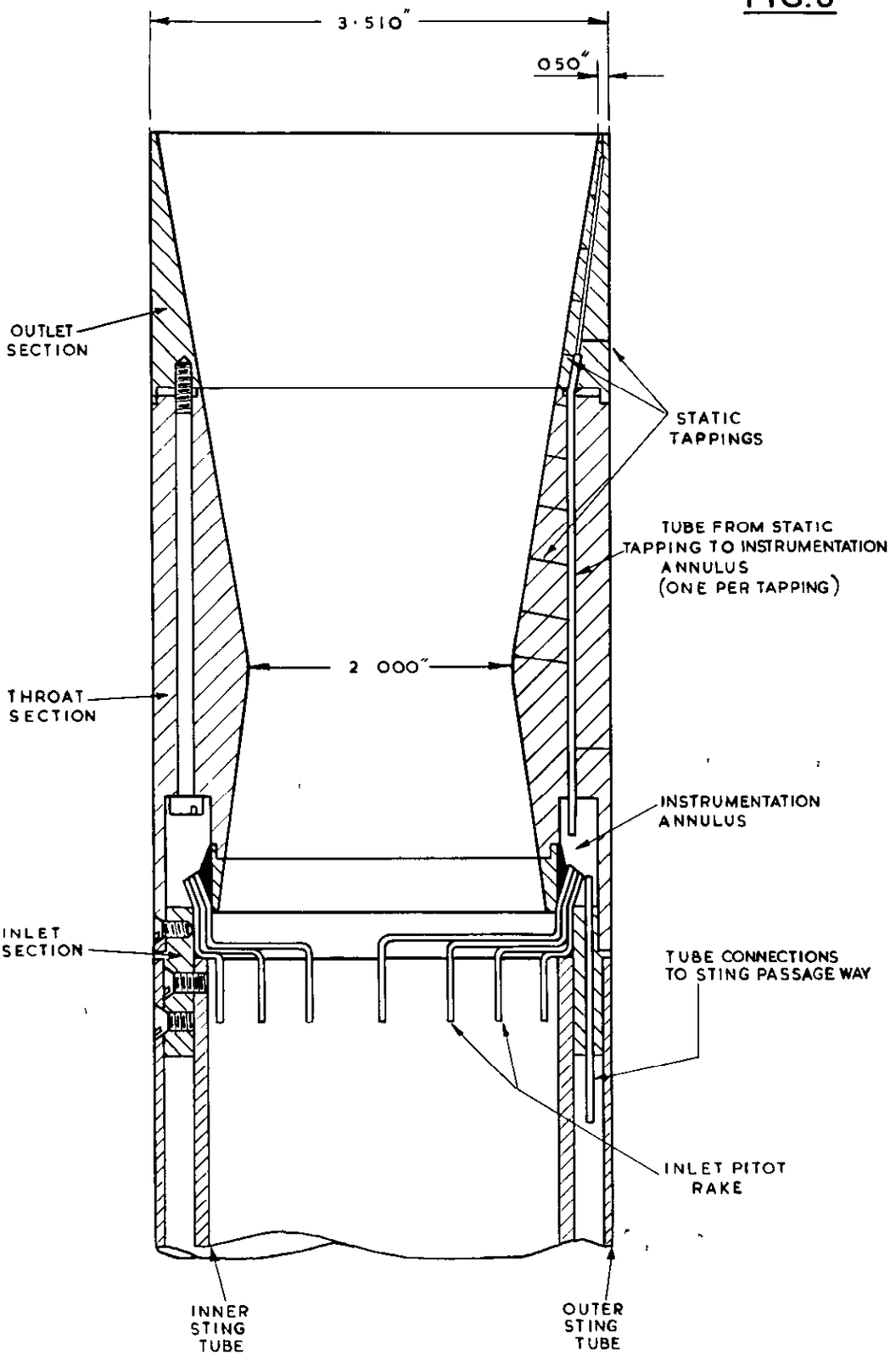

ARRANGEMENT OF MODEL PROPELLING NOZZLE

REFERENCES

No.	Author(s)	Title, etc.
1	G. T. Golesworthy	Unpublished M.O.A. Report.
2	G. T. Golesworthy	Unpublished M.O.A. Report.
3	R. J. Herd G. T. Golesworthy	The performance of a centrebody propelling nozzle with a parallel shroud in external flow - Part I. A.R.C. C.P. 841. November, 1963.
4	M. V. Herbert R. J. Herd	Boundary layer separation in supersonic propelling nozzles. A.R.C. R. & M. 3421. August, 1964.
5	M. V. Herbert D. L. Martlew	The design-point performance of model internal-expansion propelling nozzles with area ratios up to 4. A.R.C. R. & M. 3477. December, 1963.

APPENDIX

Symbols and definitions

A^* isentropic throat area

A_g geometric throat area

A_e geometric plane outlet area

A_s surface area

C_D discharge coefficient = $\dfrac{\text{actual air mass flow}}{\text{isentropic air mass flow for the same physical throat area}} = \dfrac{A^*}{A_g}$

K flow parameter = $\dfrac{Q\sqrt{T_t}}{A^* P_t}$

M_∞ freestream Mach number

P_t model entry total pressure

P_b model base pressure

P_w model internal wall pressure

P_∞ freestream static pressure

Q mass flow

R pressure ratio (see A.P.R. and E.P.R.)

Re^* model throat Reynolds number (based on throat diameter and sonic conditions)

T_t model entry total temperature

v isentropic velocity

η_F gross thrust efficiency = $\dfrac{\text{measured gauge thrust at given pressure ratio R}}{\text{gauge thrust of an isentropic nozzle, passing the same flow, at the same pressure ratio R, and fully expanded}}$

μ vacuum stream thrust efficiency at the throat

τ shear stress at wall

ϕ friction correction term = $\dfrac{\int \tau \, d(A_s)}{A_g P_t}$

A.P.R. applied pressure ratio = $\dfrac{\text{model entry total pressure}}{\text{model base pressure}} = \dfrac{P_t}{P_b}$

E.P.R. exhaust pressure ratio = $\dfrac{\text{model entry total pressure}}{\text{freestream static pressure}} = \dfrac{P_t}{P_\infty}$

FIG. I.

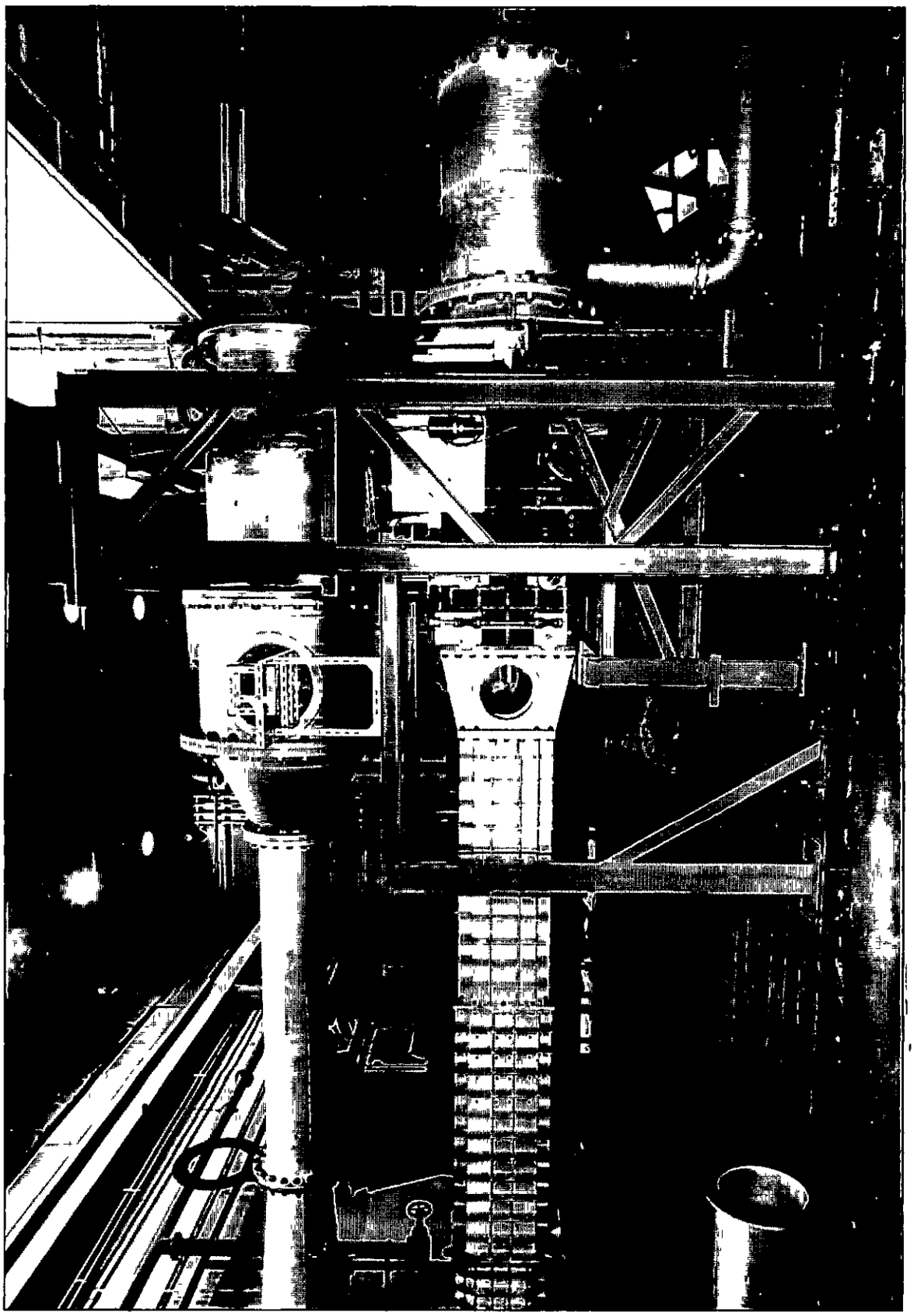

MODEL PROPELLING NOZZLE TEST RIG.

FIG.2

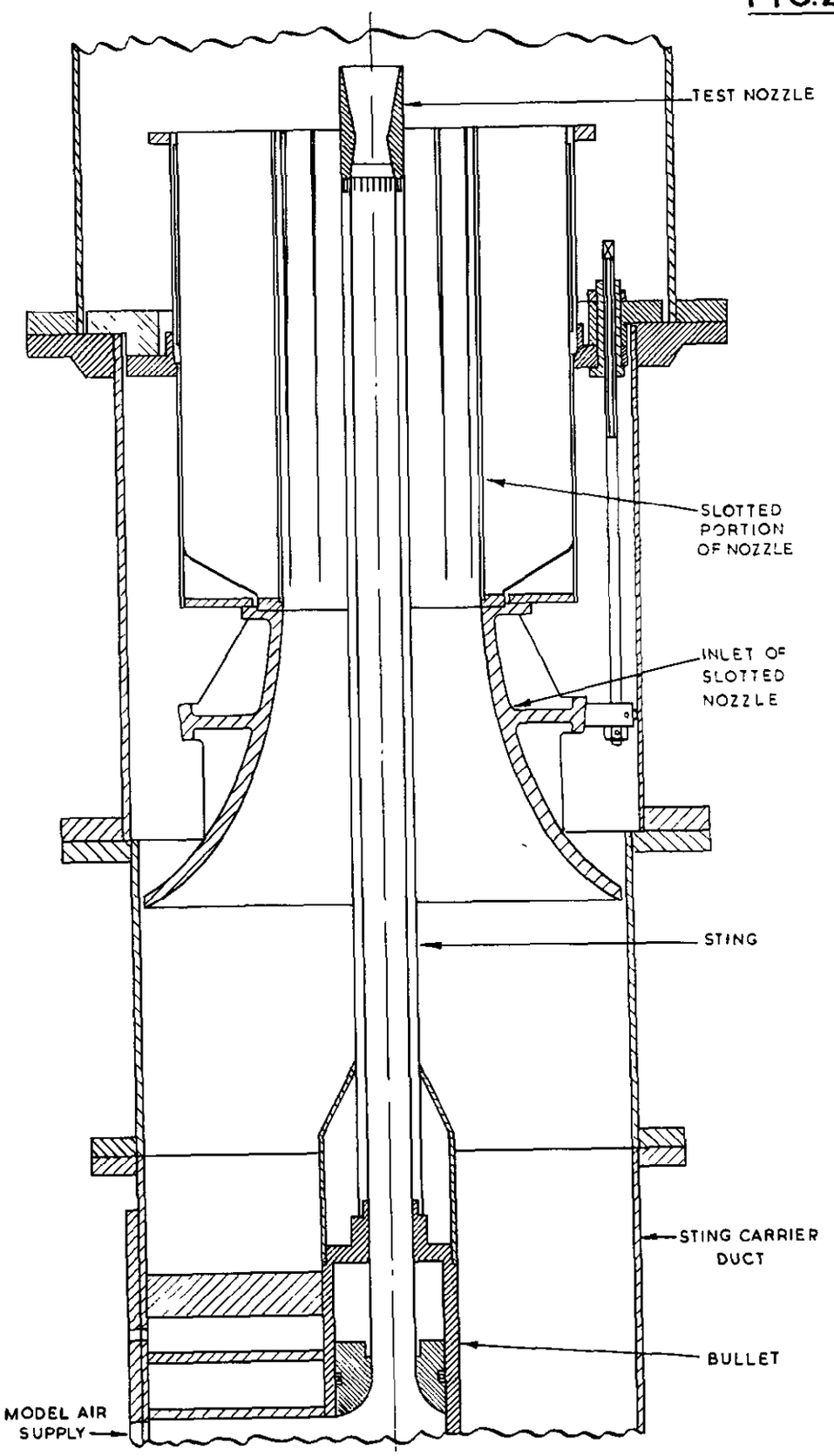

CROSS SECTION OF MODEL IN TRANSONIC EXTERNAL FLOW.

FIG.3

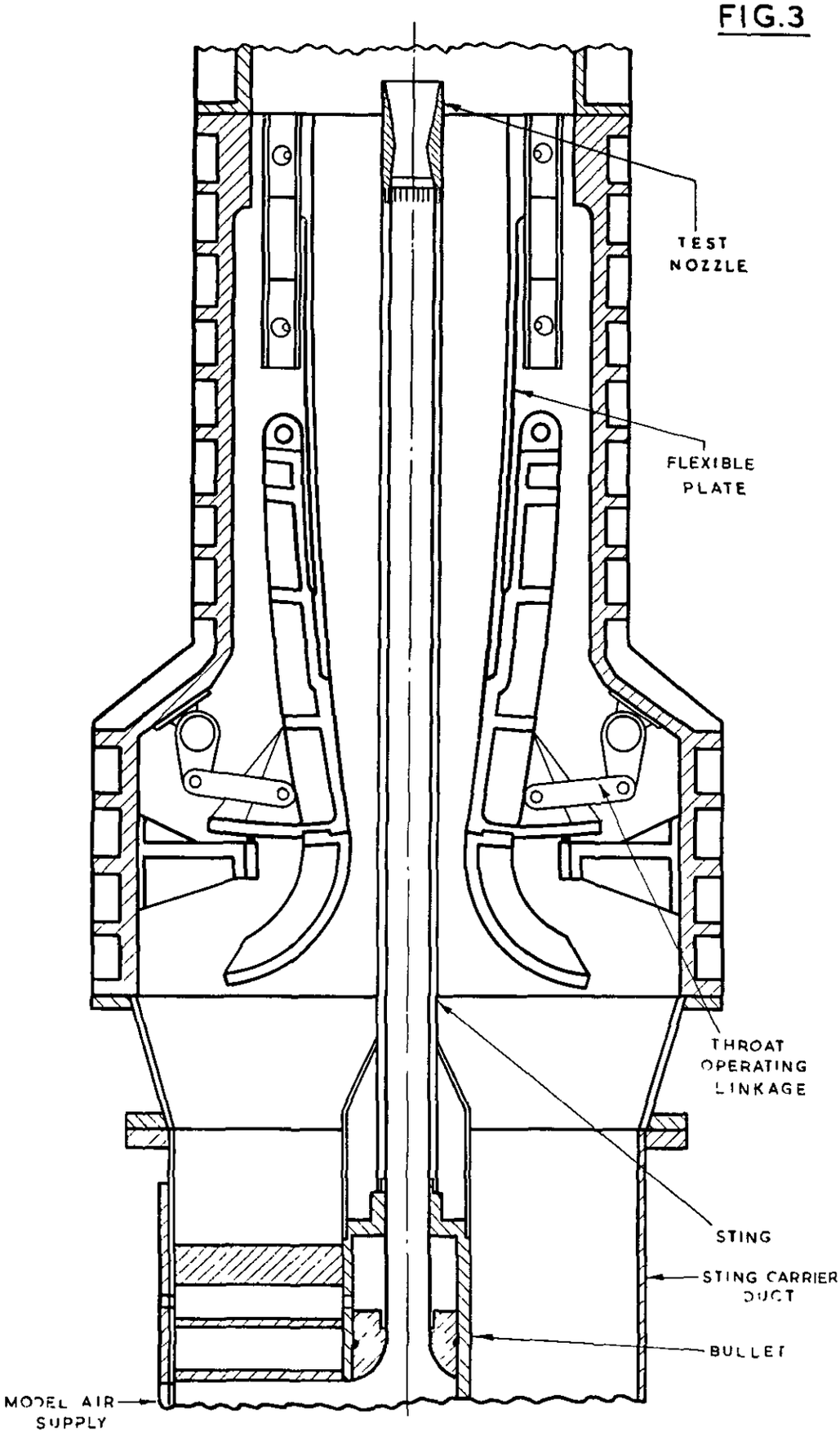

CROSS SECTION OF MODEL IN
SUPERSONIC EXTERNAL FLOW.

FIG.4

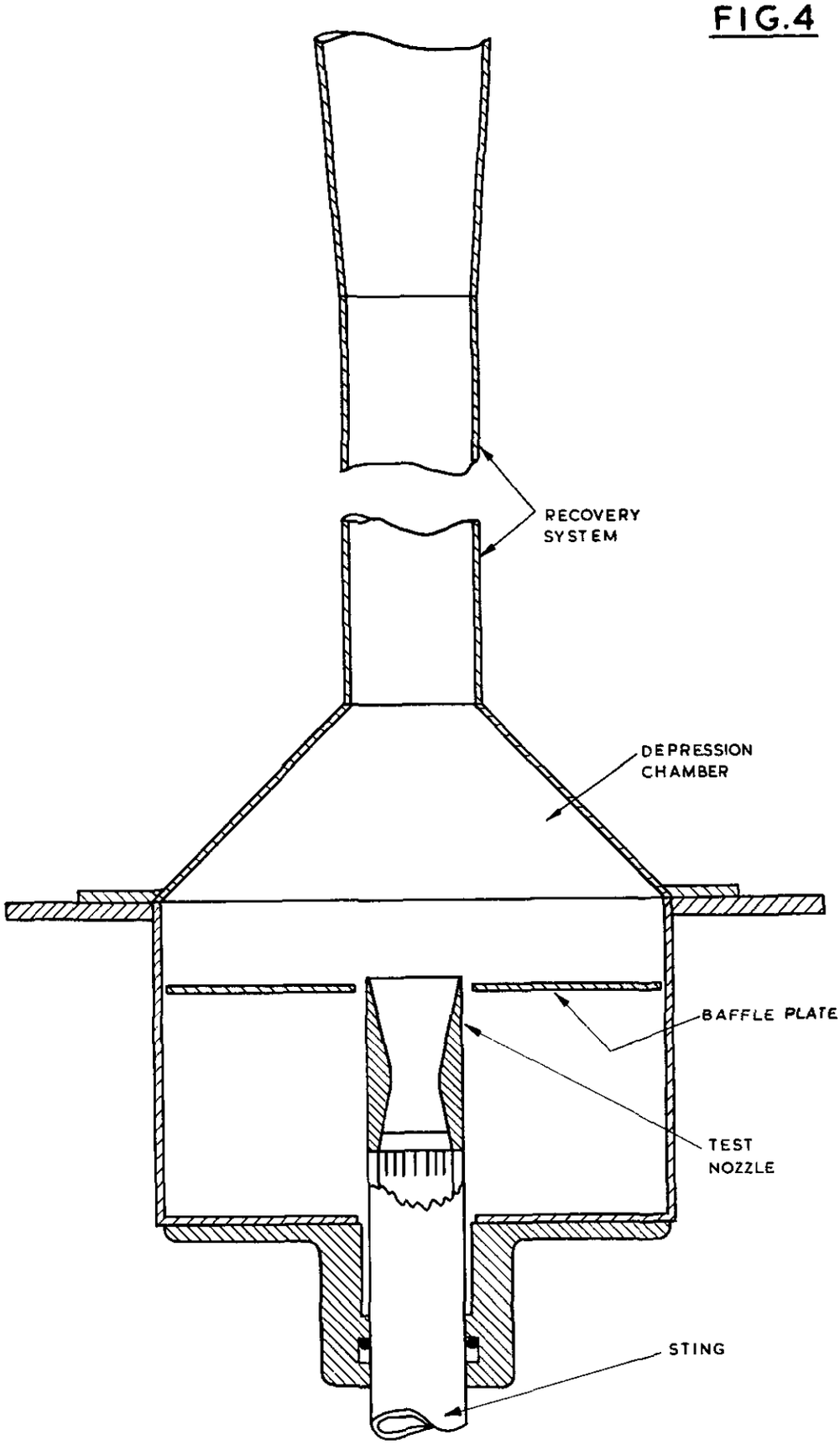

CROSS SECTION OF MODEL IN QUIESCENT AIR.

FIG. 5

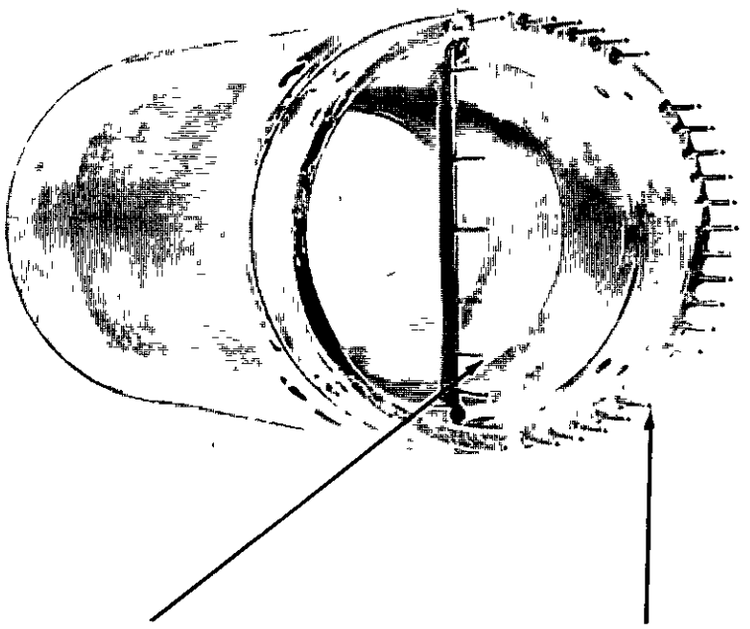

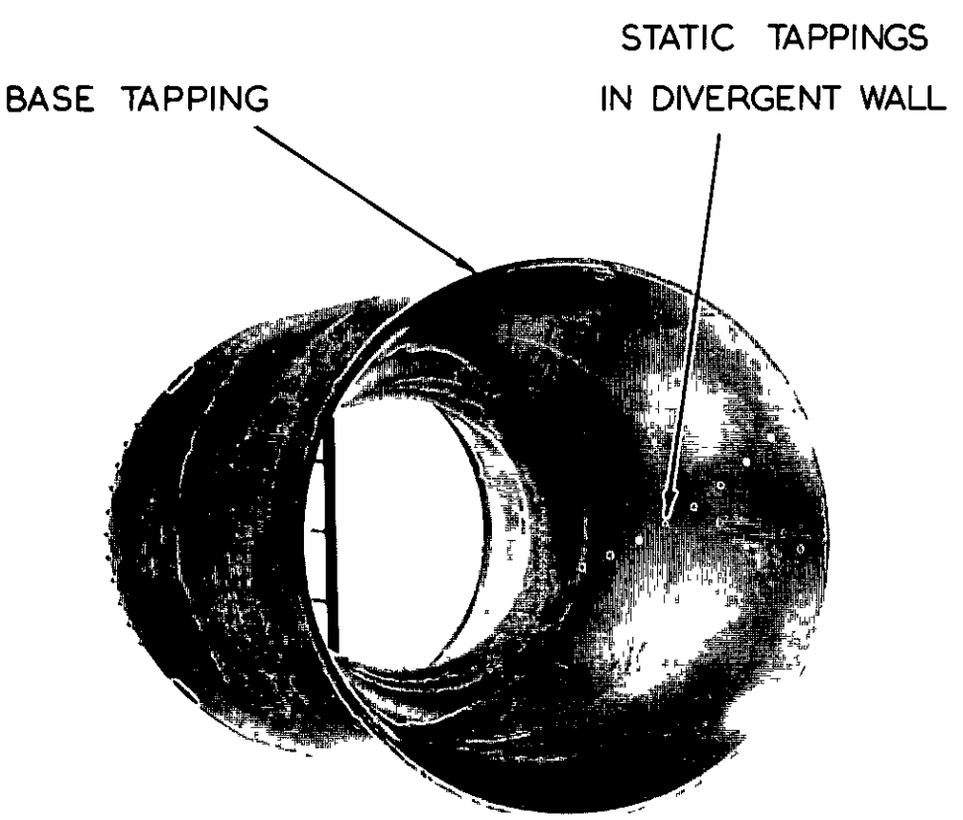

MODEL PROPELLING NOZZLE

FIG.6

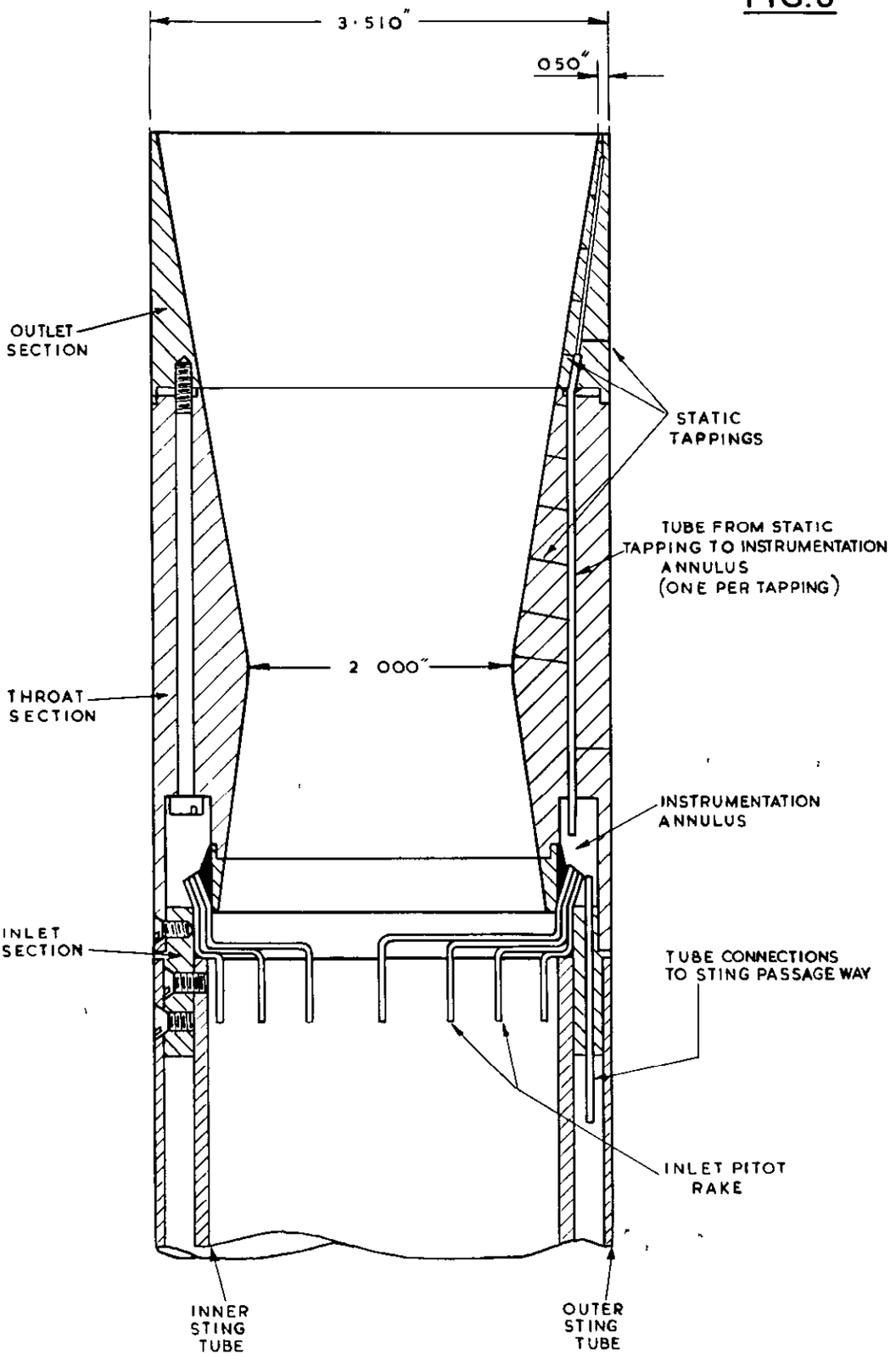

ARRANGEMENT OF MODEL PROPELLING NOZZLE

FIG.7

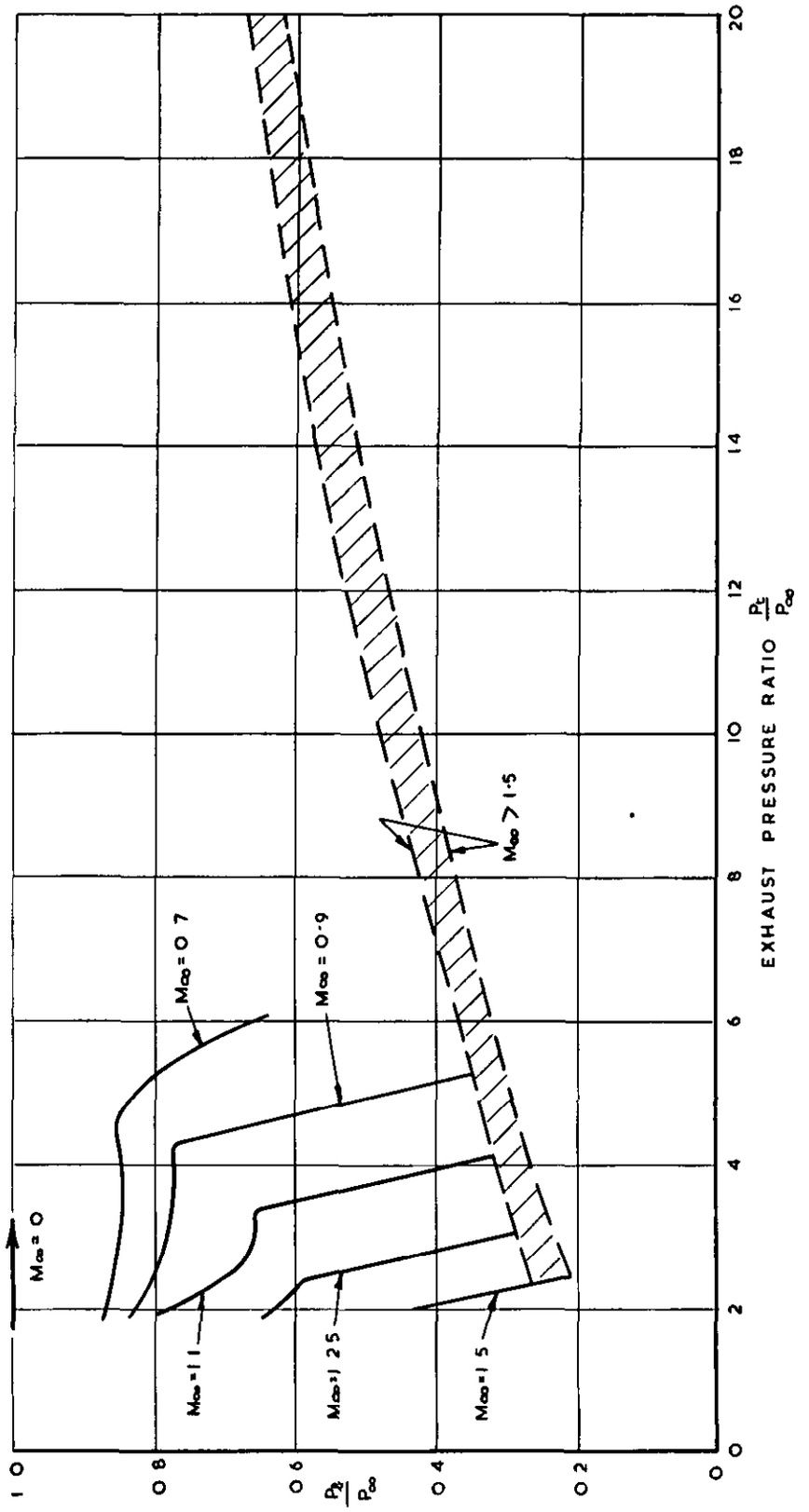

BASE PRESSURE RATIO

FIG.8

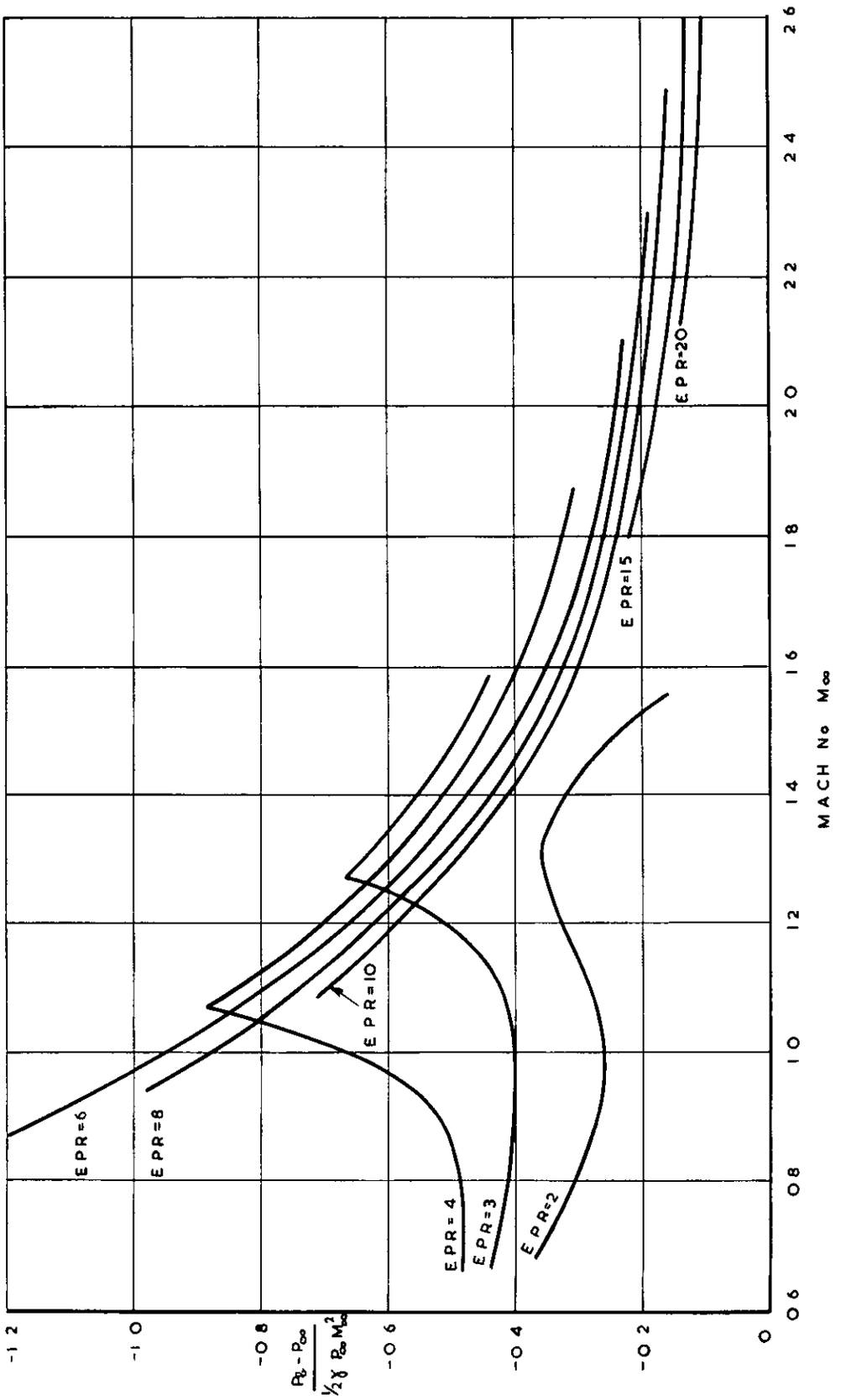

BASE PRESSURE COEFFICIENT

FIG.9.

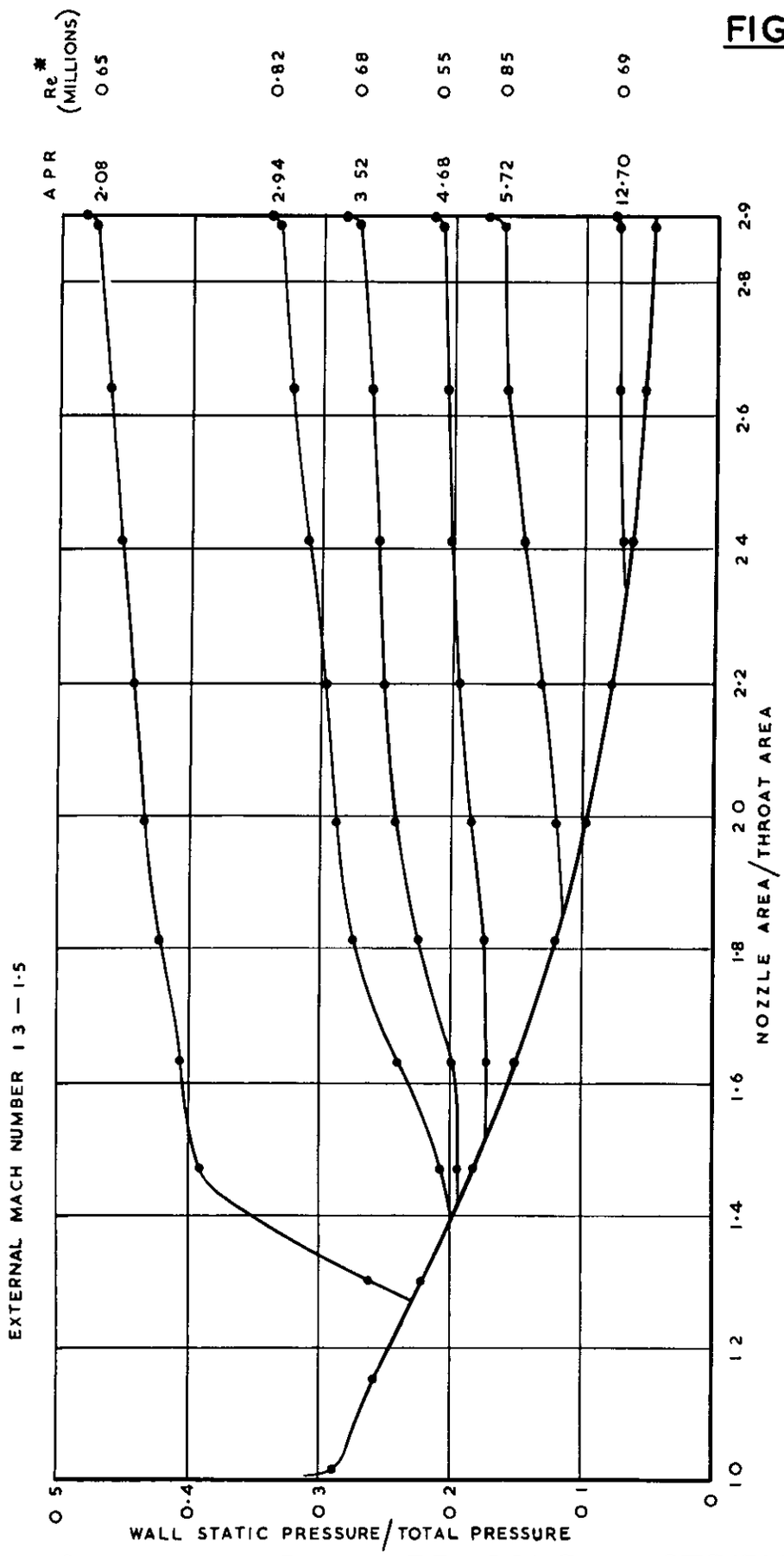

MODEL INTERNAL PRESSURE DISTRIBUTION-
SUPERSONIC EXTERNAL FLOW.

FIG.10

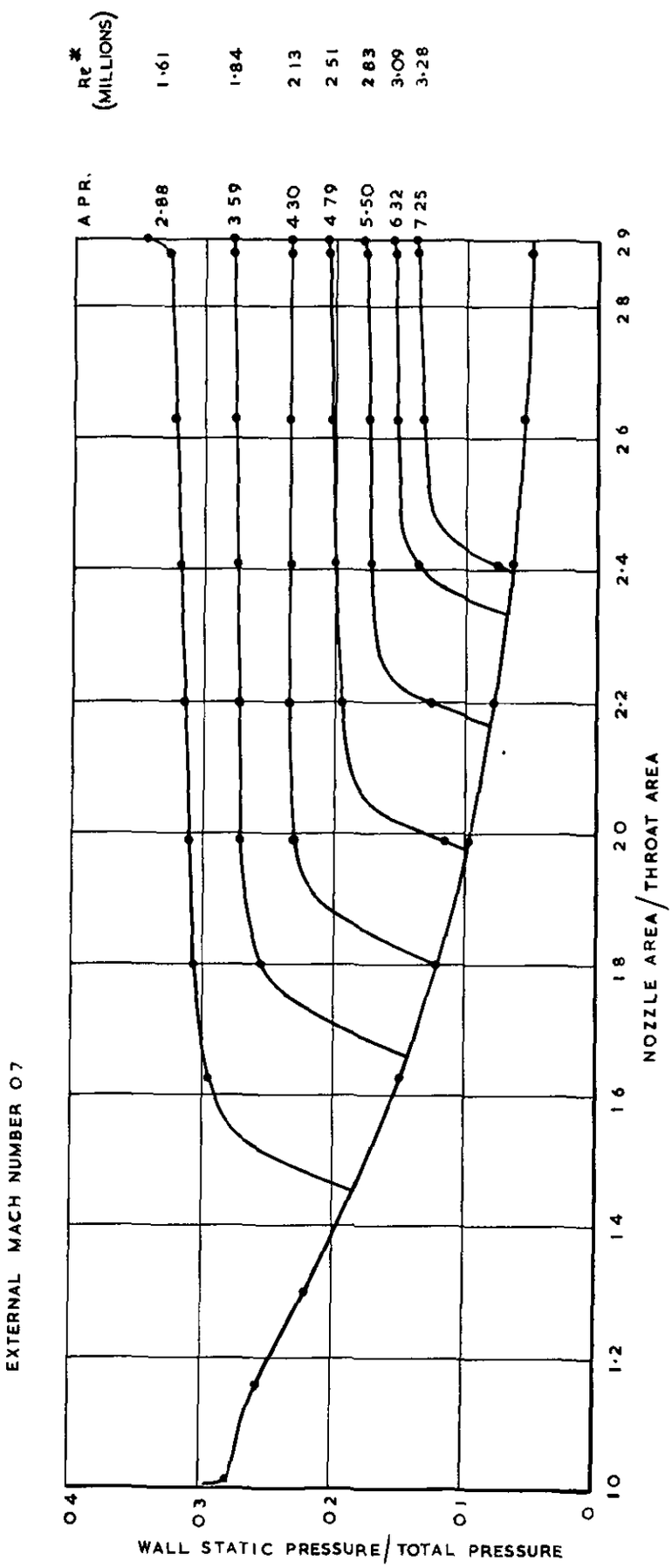

MODEL INTERNAL PRESSURE DISTRIBUTION — SUBSONIC EXTERNAL FLOW.

FIG.11

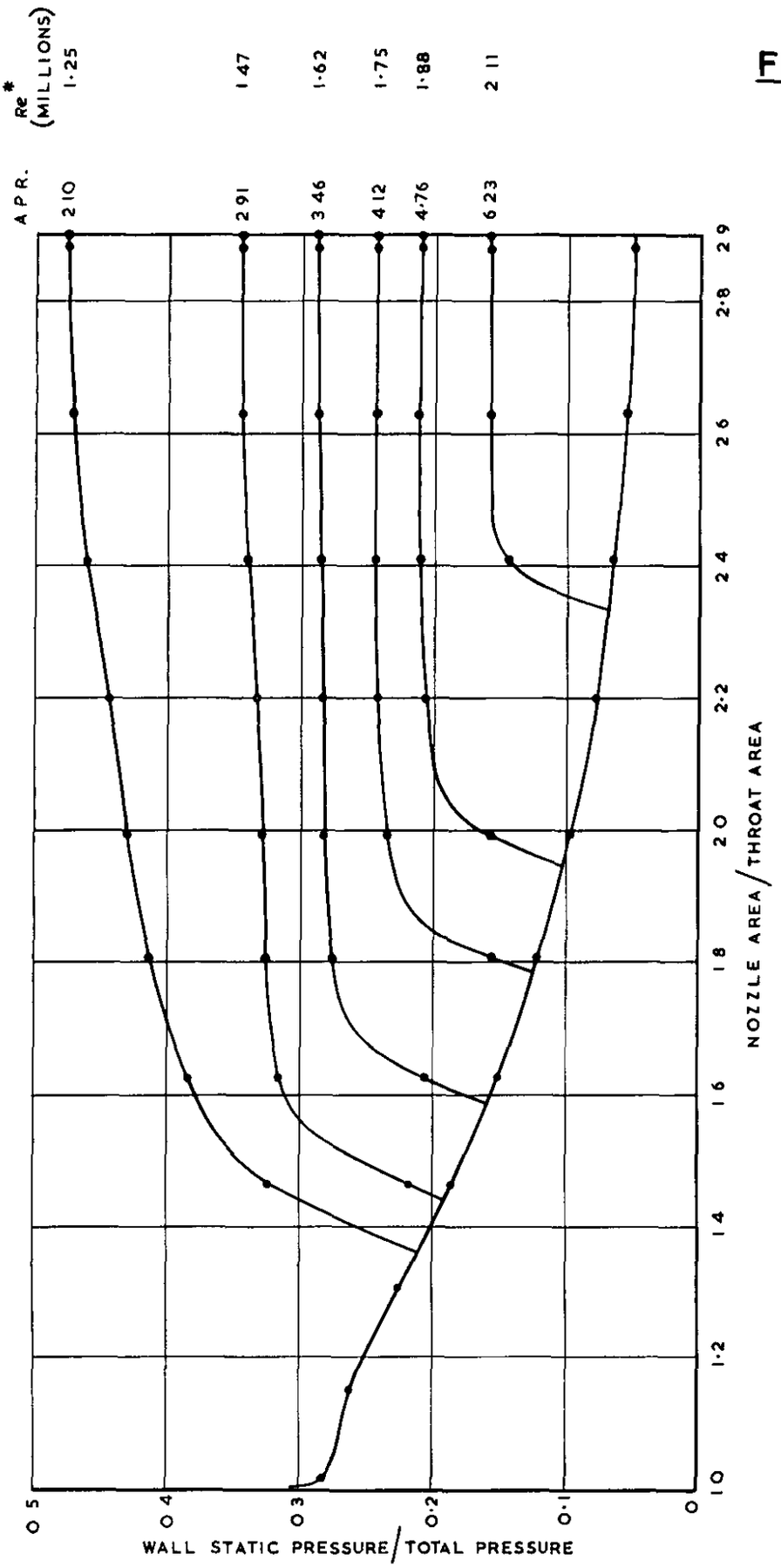

MODEL INTERNAL PRESSURE DISTRIBUTION - QUIESCENT AIR.

FIG.12

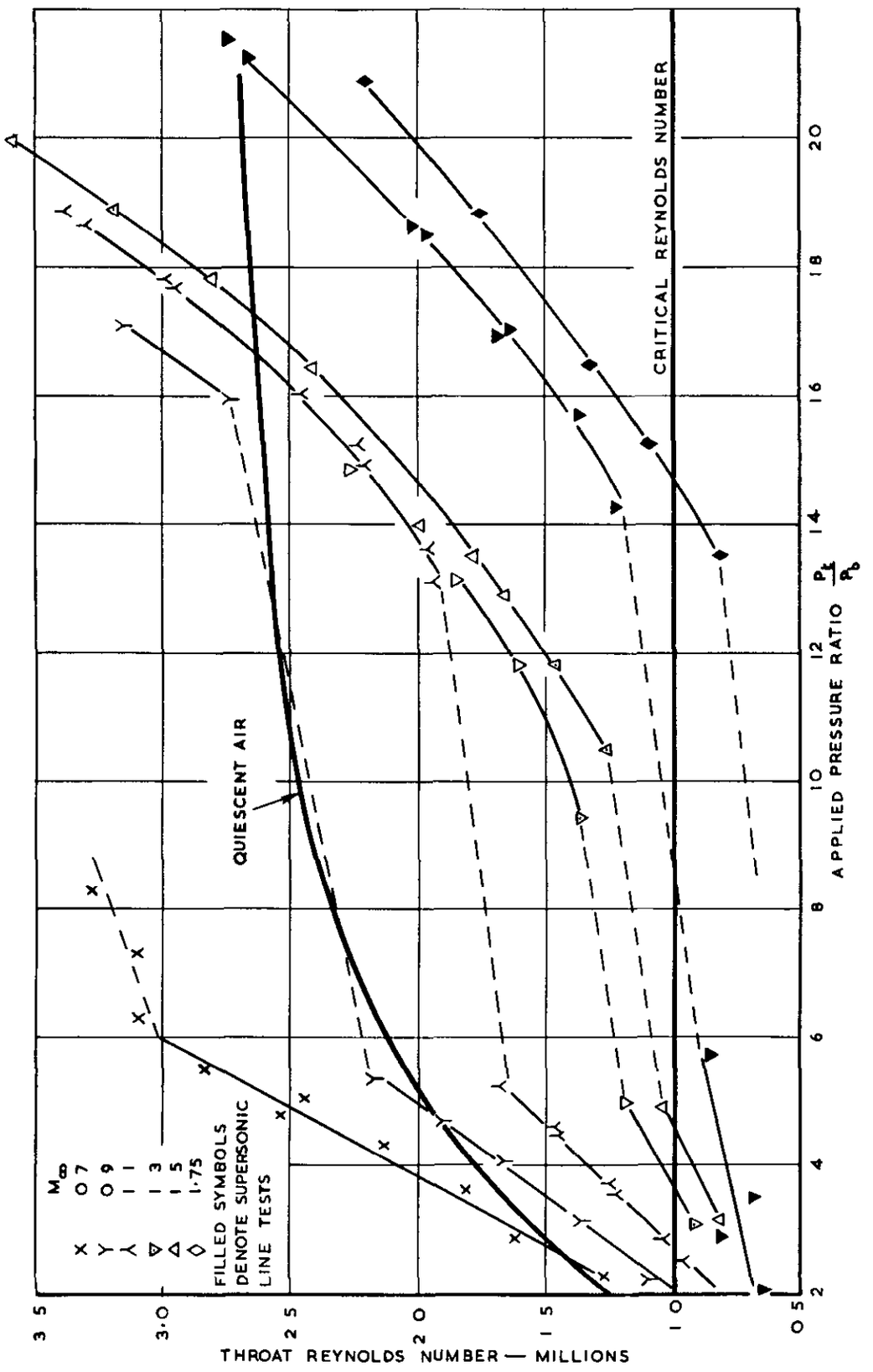

MODEL THROAT REYNOLDS NUMBER

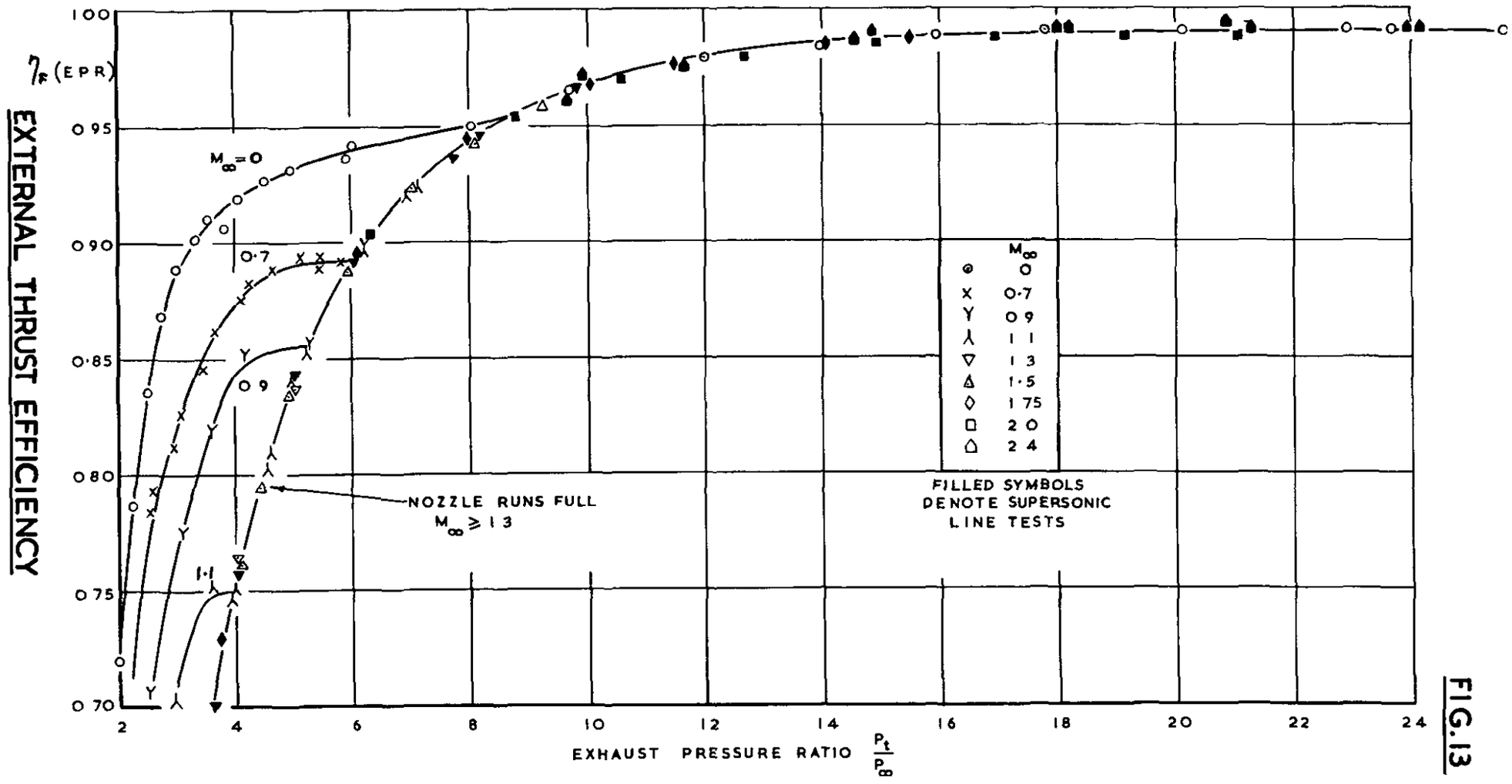
EXTERNAL THRUST EFFICIENCY
η_e (EPR)
1 00
0 95
0 90
0·85
0 80
0 75
0 70
2
4
6
8
10
12
14
16
18
20
22
24
EXHAUST PRESSURE RATIO $\frac{P_t}{P_\infty}$
$M_\infty = 0$
0·7
0 9
1·1
NOZZLE RUNS FULL
$M_\infty \geq 1\,3$
M_∞
0
0·7
0 9
1 1
1 3
1·5
1 75
2 0
2 4
FILLED SYMBOLS
DENOTE SUPERSONIC
LINE TESTS

FIG.13

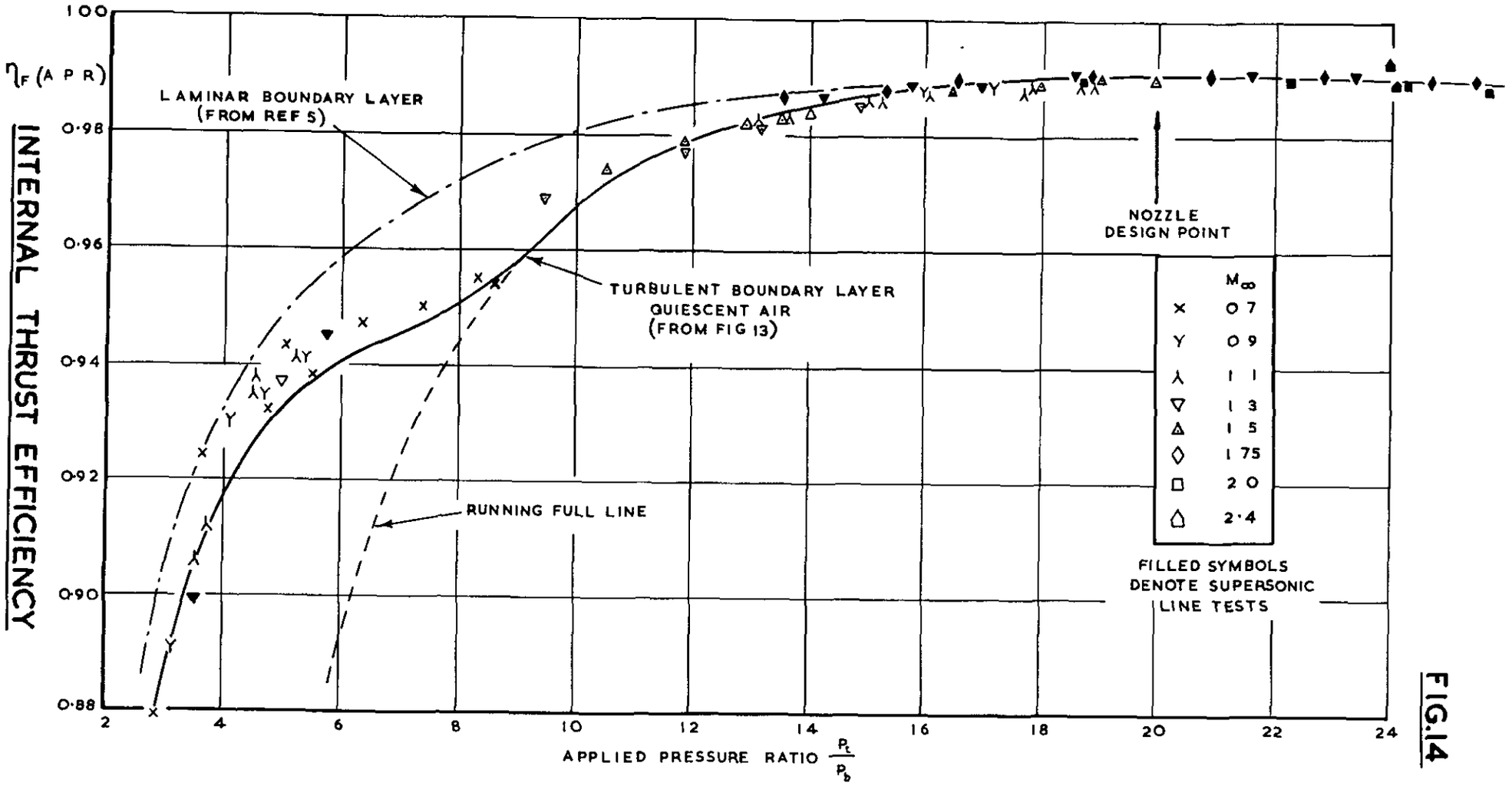
INTERNAL THRUST EFFICIENCY
η_F (A P R)
1·00
0·98
0·96
0·94
0·92
0·90
0·88
2
4
6
8
10
12
14
16
18
20
22
24
APPLIED PRESSURE RATIO $\frac{P_t}{P_b}$
LAMINAR BOUNDARY LAYER
(FROM REF 5)
TURBULENT BOUNDARY LAYER
QUIESCENT AIR
(FROM FIG 13)
RUNNING FULL LINE
NOZZLE
DESIGN POINT
M_∞
0·7
0·9
1·1
1·3
1·5
1·75
2·0
2·4
FILLED SYMBOLS
DENOTE SUPERSONIC
LINE TESTS

FIG.14

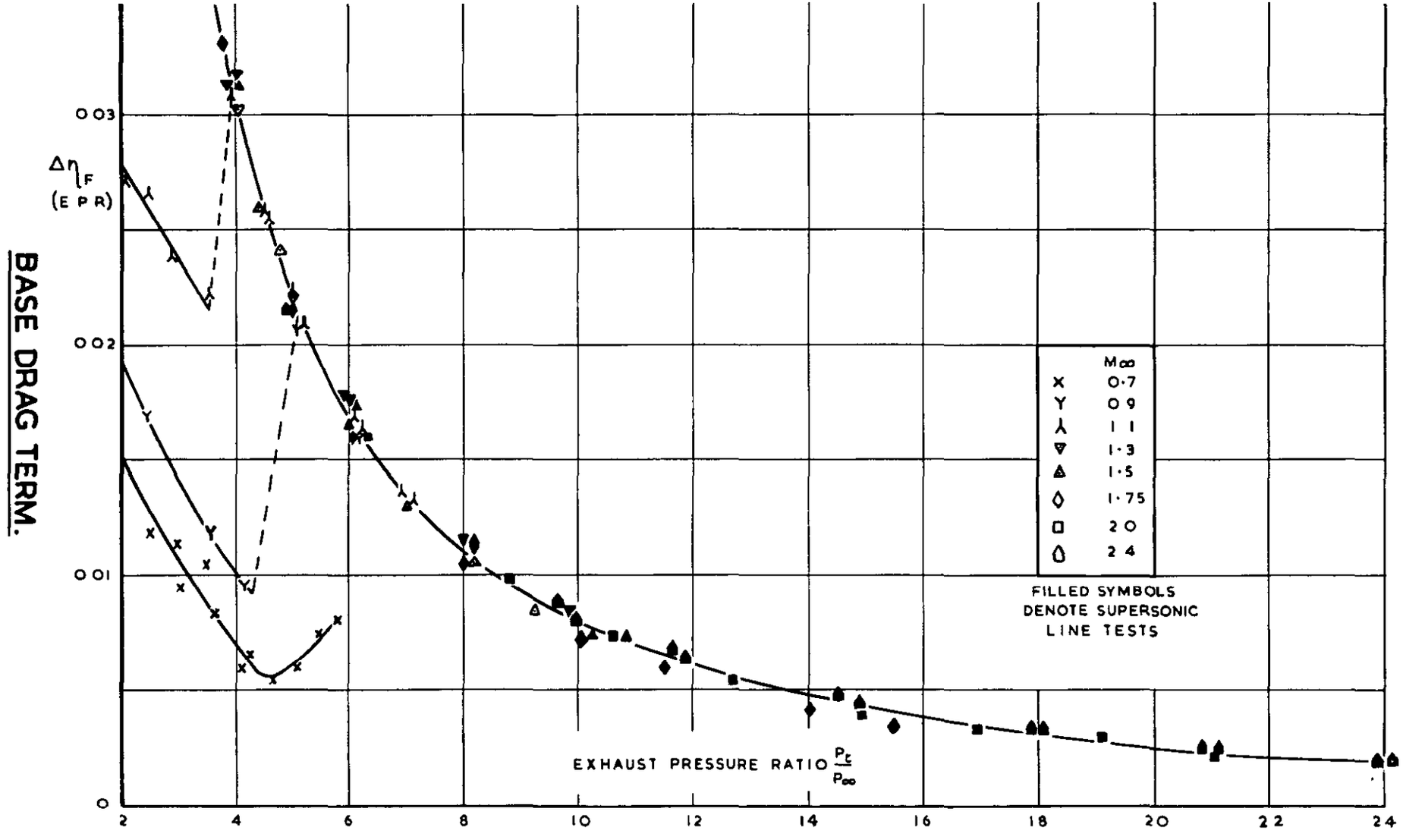
BASE DRAG TERM.
$\Delta\eta_F$ (E P R)
0 03
0 02
0 01
0
2
4
6
8
10
12
14
16
18
20
22
24
EXHAUST PRESSURE RATIO $\frac{P_t}{P_\infty}$
M∞
× 0·7
Y 0 9
1 1
1·3
1·5
1·75
2 0
2 4
FILLED SYMBOLS
DENOTE SUPERSONIC
LINE TESTS

FIG.15

A.R.C. C.P. No. 891
November, 1963
Golesworthy, G. T. and Herbert, M. V.

THE PERFORMANCE OF A CONICAL CONVERGENT-DIVERGENT NOZZLE WITH AREA RATIO 2·9 IN EXTERNAL FLOW

A model internal-expansion propelling nozzle with conical divergence of 10° semi-angle, area ratio 2·9 (design pressure ratio 20), parallel afterbody and thin annular base, has been tested both in quiescent air and in external flow over the range of Mach No. 0·7 to 2·4. Measurements have been made of nozzle base pressure, and thrust efficiencies derived with reference to both ambient and base pressure levels. Internal thrust efficiencies with external flow agree with those in quiescent air, provided that the boundary layer is in the same state in both cases.

A.R.C. C.P. No. 891
November, 1963
Golesworthy, G. T. and Herbert, M. V.

THE PERFORMANCE OF A CONICAL CONVERGENT-DIVERGENT NOZZLE WITH AREA RATIO 2·9 IN EXTERNAL FLOW

A model internal-expansion propelling nozzle with conical divergence of 10° semi-angle, area ratio 2·9 (design pressure ratio 20), parallel afterbody and thin annular base, has been tested both in quiescent air and in external flow over the range of Mach No. 0·7 to 2·4. Measurements have been made of nozzle base pressure, and thrust efficiencies derived with reference to both ambient and base pressure levels. Internal thrust efficiencies with external flow agree with those in quiescent air, provided that the boundary layer is in the same state in both cases.

A.R.C. C.P. No. 891
November, 1963
Golesworthy, G. T. and Herbert, M. V.

THE PERFORMANCE OF A CONICAL CONVERGENT-DIVERGENT NOZZLE WITH AREA RATIO 2·9 IN EXTERNAL FLOW

A model internal-expansion propelling nozzle with conical divergence of 10° semi-angle, area ratio 2·9 (design pressure ratio 20), parallel afterbody and thin annular base, has been tested both in quiescent air and in external flow over the range of Mach No. 0·7 to 2·4. Measurements have been made of nozzle base pressure, and thrust efficiencies derived with reference to both ambient and base pressure levels. Internal thrust efficiencies with external flow agree with those in quiescent air, provided that the boundary layer is in the same state in both cases.

DETACHABLE ABSTRACT CARDS

Printed and published by
HER MAJESTY'S STATIONERY OFFICE
To be purchased from
49 High Holborn, London W C 1
423 Oxford Street, London W 1
13A Castle Street, Edinburgh 2
109 St Mary Street, Cardiff
Brazennose Street, Manchester 2
50 Fairfax Street, Bristol 1
35 Smallbrook, Ringway, Birmingham 5
80 Chichester Street, Belfast 1
or through any bookseller

Printed in England

C.P. No. 891

S.O. Code No 23-9016-91